Int. J. Heat Mass Transfer. Vol. 34, No. 6, pp. 1481–1489, 1991
Printed in Great Britain

0017-9310/91 $3.00+0.00

Heat transfer near a small heated protrusion on a plate

S. GHOSH MOULIC and L. S. YAO
Department of Mechanical and Aerospace Engineering, Arizona State University, Tempe, AZ 85287, U.S.A.

(*Received* 5 *January* 1990 *and in final form* 12 *June* 1990)

Abstract—The results of a study of high Reynolds number convective heat transfer from a small heated protrusion on a flat plate are presented. Protrusions of height $\sim L\,Re^{-5/8}$ and length $\sim L\,Re^{-3/8}$ are analyzed in the context of triple-deck theory. An analytical solution for the local heat transfer rate is presented for protrusions of vanishingly small heights. For protrusions of height ~ 1 on the triple-deck scale, a numerical solution is obtained. The effect of boundary layer separation on the heat transfer rate is investigated. It is found that flow separation leads to high local rates of heat transfer downstream of the separation point.

1. INTRODUCTION

THIS INVESTIGATION considers high Reynolds number convective heat transfer from a small heated protrusion on a flat surface. This is a model to study the cooling of electronic chips. The presence of a protuberance can produce significant local changes in the flow past a flat plate and alter the local heat transfer rates appreciably. If the size of the protuberance is large, boundary layer separation may occur. The induced mixing due to boundary layer separation may result in a significant enhancement of heat transfer.

The flow structure in the vicinity of a small protrusion located at a distance L from the leading edge of a flat plate may be predicted by triple-deck theory [1–3] if the streamwise length of the protrusion is $O(L\varepsilon^3)$ and its height is $O(L\varepsilon^5)$ where $\varepsilon = Re^{-1/8}$ [4]. The protrusion or hump may then be taken as an $O(1)$ disturbance within the lower deck of a triple-deck structure. The presence of the hump results in a rapid change in the boundary layer thickness. This displacement effect produces first-order perturbations in the inviscid region just outside the boundary layer (upper deck) that interact with the viscous region close to the hump (lower deck) via the main deck (outer part of the boundary layer) to induce a streamwise pressure gradient which drives the lower deck flow. The flow in the lower deck is described by the boundary layer equations but with an induced pressure gradient which allows the flow to adjust upstream of the hump. The wall boundary conditions are the usual no-slip and kinematic boundary conditions, but the condition at the outer edge of the lower deck comes from matching to the rotational inviscid main deck, rather than the irrotational inviscid upper deck. The main deck is in turn matched to the upper deck and thus plays the passive role of transmitting streamline displacement from the lower deck to the upper deck and pressure perturbations from the upper deck to the lower deck. The triple-deck structure provides a consistent description of this self-sustaining interaction between the induced pressure gradient and streamline displacement. The importance of the triple-deck scaling has been discussed in detail by Smith [4].

The induced pressure gradient may be adverse in some regions, and, if large enough, may trigger off boundary layer separation. Due to the quasi-elliptic nature of the triple-deck pressure displacement interaction, the Goldstein singularity which appears in classical boundary layer equations at separation does not occur in the lower deck equations. Thus, small-scale separated flows may be computed numerically, using the triple-deck model.

The present investigation was restricted to protrusions which fall into the triple-deck scale. The flow over a small hump on a flat plate was first analyzed in the context of triple-deck theory by Smith [4]. He obtained linearized solutions for very small humps for both subsonic and supersonic free streams. The nonlinear lower deck equations have been solved numerically by Sykes [5] using a finite difference method, and Burggraf and Duck [6] by a pseudospectral method.

In the simple model considered in this paper, the surface of the protrusion is assumed to be maintained at a uniform temperature, T_0, which is higher than the temperature T_∞ of the free stream, while the plate is assumed to be held at a uniform temperature T_1. The wall temperature distribution is thus discontinuous at the leading and trailing edges of the protrusion. The leading-order solution for temperature does not have any upstream influence on the triple-deck scale. Therefore, the singularity introduced in the solution by the discontinuity in boundary temperature is not smoothed out. It is expected that the temperature profile ahead of the discontinuity will be influenced only in a small region where axial conduction of heat is as important as transverse conduction [7, 8]. This is the region where x and y are of

NOMENCLATURE

a	displacement function
Ai	Airy function of the first kind
d	displacement function in transformed coordinates
f	surface geometry function
h	height of protrusion
k	thermal conductivity
L	length from leading edge to center of protrusion
Nu	Nusselt number
p	pressure
Pr	Prandtl number
Q	total heat transfer rate from protrusion
Re	Reynolds number
T	temperature
T_0	temperature of surface of protrusion
T_1	plate temperature
u	x-component of velocity
v	y-component of velocity
w	transformed velocity
x	axial coordinate
y	transverse coordinate
z	transformed transverse coordinate.

Greek symbols

ε	small parameter
η	transformed transverse coordinate
θ	dimensionless temperature
ξ	axial coordinate measured from leading edge of protrusion
ω	Fourier transform variable.

$O(\varepsilon^6)$, and is not considered in this paper. The leading-order solution for temperature presented here is not valid if the wall temperature is continuous, that is, if $T_1 = T_0$. The results of this investigation are applicable to subsonic forced convection and combined free–forced convection flows as the perturbation in the buoyancy force does not appear in the leading-order momentum equation.

2. FORMULATION

The triple-deck flow structure is given in detail in ref. [4] and will be described only briefly here. The physical model is shown in Fig. 1. We consider steady, laminar, incompressible flow past a flat plate, on which is situated a small protrusion at a distance L from the leading edge of the plate. Cartesian coordinates $(\bar{x}, \bar{y})$ are chosen such that the leading edge is given by $\bar{x} = -L$ and the plate is $\bar{y} = 0$. We introduce dimensionless coordinates $(x, y) = (\bar{x}/L, \bar{y}/L)$ and nondimensionalize the problem by writing the velocity components in the $\bar{x}$- and $\bar{y}$-directions as $\bar{u} = \bar{u}_\infty u$, $\bar{v} = \bar{u}_\infty v$, respectively, the pressure as $\bar{p} = \bar{p}_\infty + \frac{1}{2}\rho\bar{u}_\infty^2 p$, and the temperature as $\theta = (T - T_\infty)/(T_0 - T_\infty)$, where $\bar{u}_\infty$ is the flow speed far from the plate, ρ the density of the fluid, $\bar{p}_\infty$ and $\bar{T}_\infty$ respectively, the pressure and temperature of the free stream, and T_0 the surface temperature of the protrusion. The Reynolds number defined by $Re = \bar{u}_\infty L/\nu$, where ν is the kinematic viscosity of the fluid, is assumed to be large. It is convenient to define a small parameter $\varepsilon = Re^{-1/8}$. Following Smith [4], we consider protrusions of height of $O(L\varepsilon^5)$ and the length of $O(L\varepsilon^3)$ with profiles $y = \varepsilon^5 hF(x/\varepsilon^3)$, where the function F is such that $hF(X)$ is of order one or less for all $X = x/\varepsilon^3$.

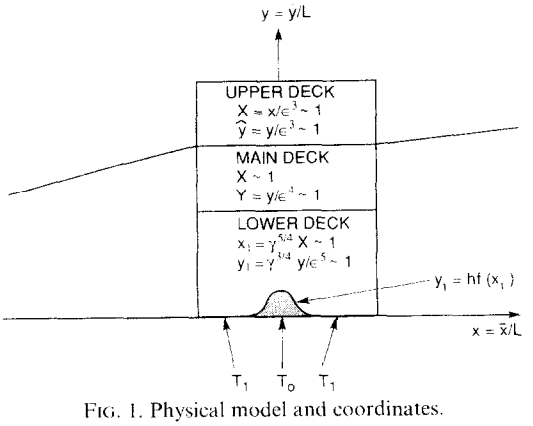

FIG. 1. Physical model and coordinates.

In the main deck, where $X = x/\varepsilon^3$ and $Y = y/\varepsilon^4$ are the $O(1)$ coordinates, the dependent variables are expanded as

$$u = U_B(Y) + \varepsilon U_1(X, Y) + \cdots$$
$$v = \varepsilon^2 V_1(X, Y) + \cdots$$
$$p = \varepsilon^2 P_1(X, Y) + \cdots$$
$$\theta = H_B(Y) + \varepsilon H_1(X, Y) + \cdots \quad (1)$$

where $U_B(Y)$ is the oncoming boundary layer velocity profile, and $H_B(Y)$ the undisturbed boundary layer temperature profile. Substitution of equations (1) into the continuity, Navier–Stokes and energy equations gives

$$\frac{\partial U_1}{\partial X} + \frac{\partial V_1}{\partial Y} = 0$$
$$U_B(Y)\frac{\partial U_1}{\partial X} + U_B'(Y)V_1 = 0$$
$$\frac{\partial P_1}{\partial Y} = 0$$
$$U_B(Y)\frac{\partial H_1}{\partial X} + H_B'(Y)V_1 = 0. \quad (2)$$

The solutions of the above equations may be written as

$$U_1 = U'_B(Y)A(X)$$
$$V_1 = -U_B(Y)A'(X)$$
$$P_1 = P_1(X)$$
$$H_1 = H'_B(Y)A(X) \quad (3)$$

where $A(X)$ is a function which has to be determined by matching.

The perturbed flow in the main deck does not match with the flow outside the boundary layer as $Y \to \infty$, and an 'upper deck' is needed to adjust the solutions to the mainstream values. In the upper deck, where $\hat{y} = y/\varepsilon^3$ and X are the relevant $O(1)$ coordinates, we expand the dependent variables as

$$u = 1 + \varepsilon^2 \hat{u}_1(X, \hat{y}) + \cdots$$
$$v = \varepsilon^2 \hat{v}_1(X, \hat{y}) + \cdots$$
$$p = \varepsilon^2 \hat{p}_1(X, \hat{y}) + \cdots$$
$$\theta = \varepsilon \hat{\theta}_1(X, \hat{y}) + \cdots. \quad (4)$$

The inviscid irrotational equations of motion yield a relation between $P_1(X)$ and $A(X)$

$$P_1(X) = \frac{1}{\pi} \int_{-\infty}^{\infty} \frac{A'(x_1)}{X - x_1} \, dx_1. \quad (5)$$

Equation (5) is a matching condition between the main deck and the upper deck. The solution for $\hat{\theta}_1$ is the trivial solution

$$\hat{\theta}_1 \equiv 0. \quad (6)$$

This is not surprising, as the temperature perturbations in the main deck satisfy the outer boundary condition as $Y \to \infty$.

The main-deck solution cannot satisfy the wall boundary conditions and so a 'lower deck' is required close to the solid surface, where X and $\hat{Y} = y/\varepsilon^5$ are the $O(1)$ coordinates. The perturbations to the upstream boundary layer solution are no longer small in this region, and the expansions take the form

$$u = \varepsilon \gamma^{1/4} u_1(x_1, y_1) + \cdots$$
$$v = \varepsilon^3 \gamma^{3/4} v_1(x_1, y_1) + \cdots$$
$$p = \varepsilon^2 \gamma^{1/2} p_1(x_1, y_1) + \cdots$$
$$\theta = \lambda + (1 - \lambda)\theta_1(x_1, y_1) + \cdots \quad (7)$$

where $\gamma = U'_B(0)$ and $x_1 = \gamma^{5/4} X$, $y_1 = \gamma^{3/4} y/\varepsilon^5$ are scaled coordinates defined for convenience, and $\lambda = (T_1 - T_\infty)/(T_0 - T_\infty)$. We also define

$$a(x_1) = \gamma^{3/4} A(X) \quad (8)$$

and

$$f(x_1) = \gamma^{3/4} F(X). \quad (9)$$

The leading-order governing equations in the lower deck are

$$\frac{\partial u_1}{\partial x_1} + \frac{\partial v_1}{\partial y_1} = 0$$
$$u_1 \frac{\partial u_1}{\partial x_1} + v_1 \frac{\partial u_1}{\partial y_1} = -\frac{\partial p_1}{\partial x_1} + \frac{\partial^2 u_1}{\partial y_1^2}$$
$$\frac{\partial p_1}{\partial y_1} = 0$$
$$u_1 \frac{\partial \theta_1}{\partial x_1} + v_1 \frac{\partial \theta_1}{\partial y_1} = \frac{1}{Pr} \frac{\partial^2 \theta_1}{\partial y_1^2}. \quad (10)$$

The boundary conditions are

$$u_1 = v_1 = 0, \theta_1 = 1 \quad \text{on } y_1 = hf(x_1)$$
$$u_1 \to y_1 + a(x_1), \theta_1 \to 0 \quad \text{as } y_1 \to \infty$$
$$u_1 \to y_1, v_1, p_1, \theta_1 \to 0 \quad \text{as } x_1 \to -\infty. \quad (11)$$

We now introduce the following transformations:

$$z_1 = y_1 - hf(x_1)$$
$$w_1 = v_1 - hu_1 f'(x_1)$$
$$d_1 = a(x_1) + hf(x_1). \quad (12)$$

Equations (10) remain unchanged in form, with z_1 and w_1 replacing y_1 and v_1, respectively. The boundary conditions become

$$u_1 = w_1 = 0, \theta_1 = 1 \quad \text{on } z_1 = 0$$
$$u_1 = z_1 + d_1(x_1) \quad \text{as } z_1 \to \infty$$
$$u_1 = z_1, v_1, p_1, \theta_1 \to 0 \quad \text{as } x_1 \to -\infty. \quad (13)$$

The lower deck equations were solved numerically for a quartic hump

$$f(x_1) = \begin{cases} (1 - x_1^2)^2, & \text{for } |x_1| < 1 \\ 0, & \text{for } |x_1| < 1 \end{cases}. \quad (14)$$

An analytical solution for the wall heat-flux distribution was also obtained for humps of very small heights, that is for $h \ll 1$.

3. LINEARIZED SOLUTION FOR THE WALL HEAT FLUX

For $h \ll 1$, the lower deck equations may be linearized by expanding the variables as

$$u_1 = z_1 + hu_{11} + O(h^2)$$
$$v_1 = hv_{11} + O(h^2)$$
$$p_1 = hp_{11} + O(h^2)$$
$$\theta_1 = \theta_{11} + O(h). \quad (15)$$

The linearized solution for the flow is given in ref. [4]. Here, we obtain a linearized solution to the lower deck energy equation. The $O(1)$ problem for temperature in the lower deck is

$$z_1 \frac{\partial \theta_{11}}{\partial x_1} = \frac{1}{Pr} \frac{\partial^2 \theta_{11}}{\partial z_1^2}$$

$$\text{at } z_1 = 0, \quad \theta_{11} = \begin{cases} 1, & -1 \leqslant x_1 \leqslant 1 \\ 0, & |x_1| > 1 \end{cases}$$

$$\text{as } z_1 \to \infty, \quad \theta_{11} \to 0$$

$$\text{as } x_1 \to -\infty, \quad \theta_{11} \to 0. \tag{16}$$

It is obvious that $\theta_{11} = 0$ for $x_1 \leqslant -1$. Since there is no upstream influence on θ_{11}, a solution may be obtained by using a Laplace transform with respect to x_1. The result for the wall temperature gradient is

$$\frac{\partial \theta_{11}}{\partial z_1}(x_1, 0) = \begin{cases} 0, & \text{for } x_1 < -1 \\ \dfrac{Ai'(0) Pr^{1/3}}{\Gamma(2/3) Ai(0)} (x_1+1)^{-1/3}, & \text{for } -1 \leqslant x_1 \leqslant 1 \\ \dfrac{Ai'(0) Pr^{1/3}}{\Gamma(2/3) Ai(0)} [(x_1+1)^{-1/3} - (x_1-1)^{-1/3}], & \text{for } x_1 > 1 \end{cases} \tag{17}$$

where Ai is the Airy function of the first kind.

Equation (17) indicates that the wall heat-flux distribution is singular at the points $x_1 = \pm 1$, that is, at the leading and trailing edges of the hump. At the leading edge $x_1 = -1$, the thermal boundary layer has zero thickness. Therefore, the wall heat flux is infinite. This implies the existence of a small region near the leading edge where axial conduction of heat cannot be neglected [7, 8]. The thermal boundary layer near the trailing edge $x_1 = 1$ has a double structure. Due to the sudden change in boundary temperature at $x_1 = 1$ there exists a thin sublayer of thickness $O((x_1-1)^{1/3})$ near the wall where the temperature gradient in the transverse direction is large.

4. THE NUMERICAL METHOD

The leading-order velocity perturbations in the lower deck were computed by a hybrid spectral finite-difference method. The solution procedure is based on that of Burggraf and Duck [6]. The pressure gradient term in the momentum equation is eliminated by differentiating it with respect to z, and the solution variables are split into two components, namely, that corresponding to uniform shear ($u_1 = z_1$) and a perturbation component. We also map the semi-infinite interval $0 \leqslant z_1 < \infty$ to a finite interval by a transformation $z_1 = g(t)$. The resulting transport equation for the perturbation shear stress is then transformed from physical to spectral variables using the Fourier integral transform in x_1. This yields

$$\frac{1}{[g'(t)]^2} \frac{\partial^2 \tilde{\tau}^*}{\partial t^2} - \frac{g''(t)}{[g'(t)]^3} \frac{\partial \tilde{\tau}^*}{\partial t} - i\omega g(t) \tilde{\tau}^* = R^* \tag{18}$$

where

$$R = \tilde{u}_1 \frac{\partial \tilde{\tau}}{\partial x} + \frac{t}{g'(t)} \frac{\partial \tilde{\tau}}{\partial t}$$

$$\tilde{\tau} = \frac{1}{g'(t)} \frac{\partial \tilde{u}_1}{\partial t}. \tag{19}$$

Here, perturbation components are denoted by a tilde, while an asterisk denotes a transformed variable, e.g.

$$\tilde{\tau}^*(\omega, t) = \int_{-\infty}^{\infty} \tilde{\tau}(x, t) e^{-i\omega x} \, dx. \tag{20}$$

The boundary conditions applied to equation (18) are

at $t = 0$,

$$\frac{\partial \tilde{\tau}^*}{\partial t} \to -i\omega |\omega| g'(t) \left[h f^*(\omega) - \int_0^t \tilde{\tau}^*(\omega, t') \, dt' \right]$$

$$\text{as } t \to t_\infty, \quad \tilde{\tau}^* \to 0. \tag{21}$$

This system of equations was solved by a finite-difference method. Central differences were applied on the t-derivatives in equation (18). The t-derivative in the interaction condition in equation (21) was replaced by a three-point backward difference formula. Quadratures were evaluated using the trapezoidal rule. The function $g(t)$ was taken to be

$$g(t) = \frac{t}{1-t}. \tag{22}$$

Uniform steps $\Delta t = t_\infty/(J-1)$ in t, where J is the number of points in the t-direction, correspond to non-uniform steps Δz_1 in z_1. Transformation (22) has the property that points are concentrated close to the solid boundary $z_1 = 0$. The grid spacings $\Delta\omega$ and Δx_1 were chosen to satisfy the relation

$$\Delta x_1 \Delta \omega = \frac{2\pi}{K} \tag{23}$$

where K is the number of points in the x_1-direction. The range of x_1 was truncated to

$$-\frac{K}{2} \Delta x_1 \leqslant x \leqslant \left(\frac{K}{2} - 1 \right) \Delta x_1$$

while the range of ω was truncated to

$$-\frac{K}{2} \Delta \omega \leqslant \omega \leqslant \left(\frac{K}{2} - 1 \right) \Delta \omega.$$

Relation (23) allows fast transformation of variables from the physical space to spectral space, and vice versa, using the fast Fourier transform technique of Cooley and Tukey [9]. Aliasing errors in the evaluation of the convolution product R^* were removed by padding or truncation [10].

After several trials, t_∞ was fixed at 0.95 and Δx was

set to 0.0625. J and K were taken to be 61 and 512, respectively.

Since the wall boundary temperature is discontinuous, its discrete Fourier transform exhibits the Gibbs phenomenon. To avoid this problem, the lower deck energy equation was solved in the physical plane. The leading-edge singularity was removed by the following transformation:

$$\xi = x_1 + 1$$

$$\eta = \frac{y}{\xi^{1/3}}. \tag{24}$$

In (ξ, η) coordinates, the lower deck energy equation has the form

$$\xi^{2/3} u_1 \frac{\partial \theta_1}{\partial \xi} + \left(\xi^{1/3} v - \frac{\eta u_1}{3\xi^{1/3}}\right)\frac{\partial \theta_1}{\partial \eta} = \frac{1}{Pr}\frac{\partial^2 \theta_1}{\partial \eta^2}. \tag{25}$$

The boundary conditions are

$$\text{at} \quad \eta = 0, \quad \theta_1 = \begin{cases} 1, & 0 \leqslant \xi \leqslant 2 \\ 0, & \xi > 2 \end{cases}$$

$$\text{as} \quad \eta \to \infty, \quad \theta_1 = 0. \tag{26}$$

At $\xi = 0$, equation (25) reduces to

$$\frac{\partial^2 \theta_1}{\partial \eta^2} + \frac{\tau_0 Pr}{3}\eta^2 \frac{\partial \theta_1}{\partial \eta} = 0 \tag{27}$$

where τ_0 is the wall shear stress at $\xi = 0$. The initial conditions for equation (25) were generated by solving equation (27) subject to boundary conditions (26).

Equation (25) was solved by a finite-difference method. The interval $0 \leqslant \eta < \infty$ was mapped to the finite interval $0 \leqslant t < 1$ by equation (22). The t-derivatives were discretized by central differences, while the ξ-derivative in equation (25) was approximated by a two-point upwind difference scheme. For flows without separation, the upwind difference scheme is equivalent to a backward difference scheme, and the solution is obtained in a single sweep by marching from $\xi = 0$. For separated flows, several sweeps in the ξ-direction are required.

The numerical solution obtained is not accurate near $\xi = 2$ because of the discontinuity in boundary temperature. The thermal boundary layer near $\xi = 2$ has a double structure, as indicated by the linearized solution. For flows without separation, this singularity may be accounted for by a two-region method [11, 12]. For flows with separation, however, this two-region method fails [12], and hence was not used in this investigation. The numerical results obtained for the local heat transfer rate for the limiting case $h = 0$ were compared with the analytical result given by equation (17) in Fig. 2 for $Pr = 1$. As expected, the computed solution differs from the exact solution in the region downstream of the trailing edge x_1. However, the error introduced by the trailing edge singularity decays rapidly with distance downstream of the trailing edge, and the exact solution is recovered.

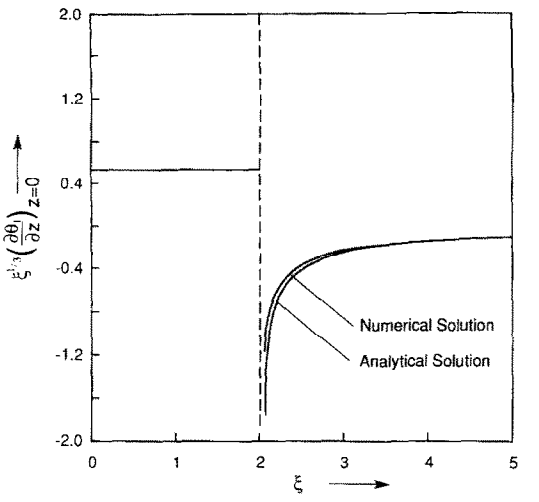

FIG. 2. Comparison of numerical solution for $h = 0$ with analytical solution.

5. RESULTS AND DISCUSSION

Numerical results were obtained for the quartic hump (equation (14)) for hump heights $h = 0.1$, 1 and 3. Details of the main-deck displacement, induced pressure and wall shear stress are presented in Figs. 3–5. Results for the heat transfer rates are presented for $Pr = 0.7$ (air) and 8 (water) in Figs. 6 and 7.

The main-deck displacement $d_1(x_1)$ is plotted in Fig. 3. Figure 3 shows that the main-deck flow decelerates ahead of the hump, reaching a minimum near the leading edge, and then accelerates along the rising portion of the hump from the leading edge to the crest, where the slope is positive. The peak of the displacement $d_1(x_1)$ occurs at the crest $x_1 = 0$ for $h = 0.1$. For humps of larger heights, the peak of the displacement function occurs slightly ahead of the crest $x_1 = 0$ due to the non-linear convection effect in the lower deck. On the leeward side of the hump, the flow decelerates rapidly to a minimum at the trailing edge. Beyond the trailing edge, the flow accelerates again, and the displacement function $d_1(x_1)$ approaches zero asymptotically from below. The range of upstream and downstream influence increases as h increases.

The induced pressure distribution is shown in Fig. 4. As expected, a favorable pressure gradient is developed in regions where the main-deck flow accelerates, while an adverse pressure gradient is developed in regions where the flow decelerates. Thus, the pressure rises gradually upstream of the hump to a maximum near the leading edge, and then decreases rapidly along the windward side of the hump, falling below the free-stream value to a minimum at the crest of the hump. On the leeward side of the hump, the pressure rises rapidly, overshooting the free-stream level, and then decreases asymptotically to zero from above far downstream of the hump. The induced pressure perturbations are larger for humps of larger heights. Figure 4 indicates that the most likely place

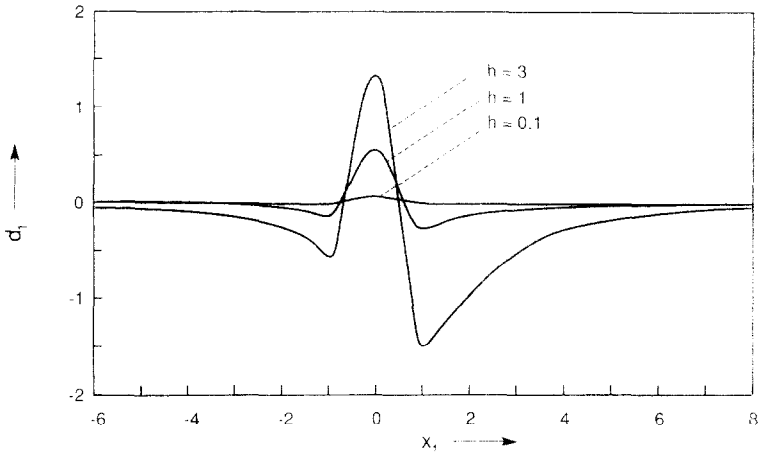

FIG. 3. Main-deck displacement.

for separation to occur is the downstream end of the hump where the induced adverse pressure gradient is greatest. This is confirmed by the wall shear-stress distribution (Fig. 5).

Figure 5 shows the wall shear-stress distribution. Upstream of the hump, the wall shear-stress decreases as the flow decelerates, to a minimum at the leading edge. Beyond the leading edge, the wall shear-stress rises drastically as the flow accelerates, reaching a maximum slightly ahead of the crest of the hump, and then decreases as the flow decelerates, to a minimum near the trailing edge of the hump. Beyond the trailing edge, the shear-stress increases and asymptotically approaches the unperturbed boundary layer solution from below. For $h = 3$, the flow separates on the leeward side of the hump, and there is a region of negative shear-stress inside the separation bubble. The curve for $h = 3$ indicates that the flow separates around $x_1 = 0.5$ and reattaches at $x_1 = 1.8$.

Figure 6(a) shows the variation of the local heat transfer rate at the wall for $Pr = 0.7$. The local Nusselt number, defined in terms of $T_0 - T_\infty$, the thermal conductivity k and the length L, can be expressed as

$$Nu = \varepsilon^{-5}\gamma^{3,4}\, Nu_1 + \cdots \tag{28}$$

where

$$Nu_1 = -\xi^{1/3}\left(\frac{\partial\theta}{\partial\eta}\right)_{\eta=0} \tag{29}$$

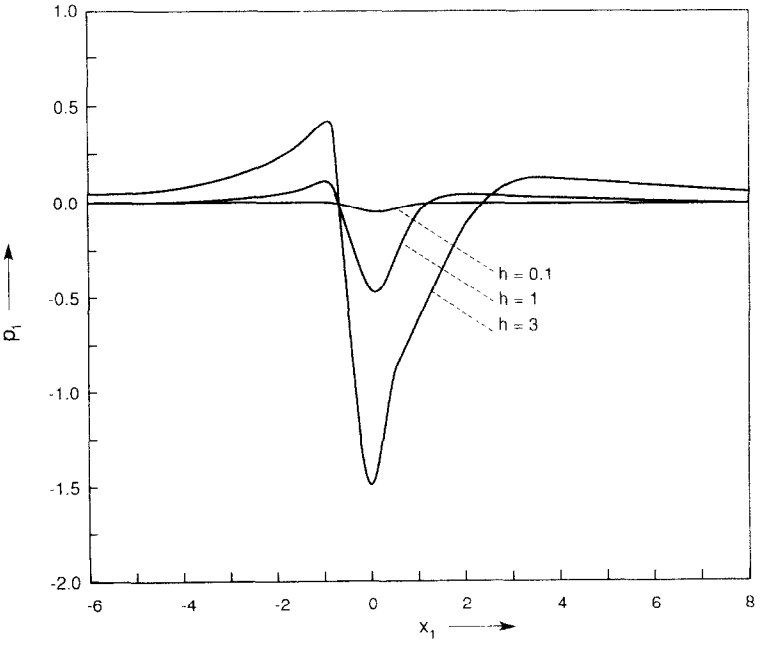

FIG. 4. Pressure distribution.

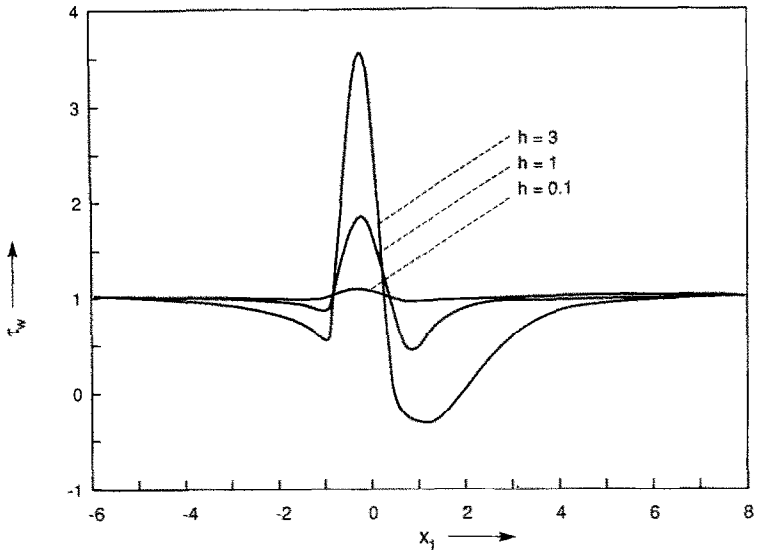

FIG. 5. Wall shear–stress distribution.

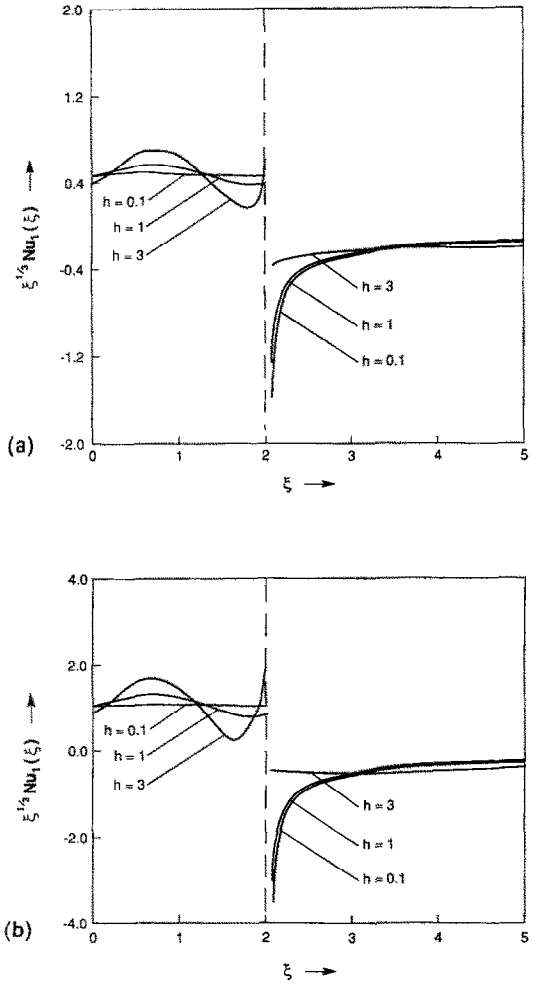

FIG. 6. (a) Local heat transfer rate for $Pr = 0.7$. (b) Local heat transfer rate for $Pr = 8$.

is obtained from the lowest order energy equation in the lower deck. Equation (29) indicates that $Nu_1 \sim \xi^{-1/3}$ near $\xi = 0$. For humps of very small heights, equation (17) predicts that $\xi^{1/3} Nu_1$ is constant along the surface of the hump, that is, in the region $0 \leqslant \xi \leqslant 2$. Thus, the axial variation of $\xi^{1/3} Nu_1$ has been plotted in Fig. 6(a), rather than the variations of Nu_1. As expected, $\xi^{1/3} Nu_1$ is very nearly constant in the region $0 \leqslant \xi \leqslant 2$ for $h = 0.1$. As the height h of the protrusion is increased, the flow decelerates ahead of the protrusion and heat is convected away from the surface at a slower rate near the leading edge. The values of $\xi^{1/3} Nu_1$ for $h = 1$ and 3 at the leading edge $\xi = 0$ are, therefore, lower than the corresponding value for $h = 0.1$. The curves for $h = 1$ and 3 show that as the fluid accelerates along the 'windward' side of the hump, the local heat transfer rate increases above the flat-plate value to a maximum slightly ahead of the center of the protrusion and decreases to a local minimum near the trailing edge as the fluid decelerates along the leeward side of the hump. For $h = 1$, the minimum occurs at the trailing edge $\xi = 2$. For $h = 3$, the flow separates ahead of the trailing edge and the minimum occurs upstream of the trailing edge, at the separation point, where the local flow is similar to a reverse-stagnation point flow. Just downstream of the separation point, the local wall heat transfer rate rises rapidly as the mixing of cold fluid with hot fluid induced by the recirculating eddy carries away heat from the surface at a faster rate. All the curves show a discontinuity in the wall heat flux at the trailing edge $\xi = 2$ due to the sudden step change in wall temperature. Downstream of the trailing edge, the wall heat flux changes sign as the hot fluid now transfers heat to the cooler wall. The magnitude of the wall heat flux is high near the trailing edge. The trailing

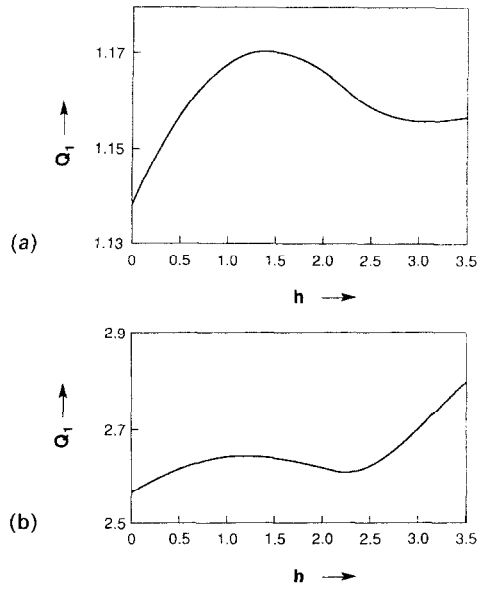

FIG. 7. (a) Total heat transfer rate from surface of protrusion for $Pr = 0.7$. (b) Total heat transfer rate from surface of protrusion for $Pr = 8$.

edge itself is a singular point, and for flows without separation, the wall heat flux is infinite at that point. Far downstream of the trailing edge, the wall heat flux decays algebraically to zero, as the thermal boundary layer grows in thickness.

Figure 6(b) shows the variation of the local heat transfer rate for $Pr = 8$. The curves follow the same trend as in Fig. 6(a). The magnitude of the local heat transfer rates are, however, larger for $Pr = 8$, as the thermal boundary layer is thinner and the temperature gradients at the wall are larger.

The total heat transfer rate, Q, from the surface of the protrusion can be obtained by integrating equation (29). It may be expressed as

$$\frac{Q}{k(T_0 - T_\infty)} = \varepsilon^{-2}\gamma^{1/2}Q_1 + \cdots \tag{30}$$

where

$$Q_1 = \int_{\xi=0}^{2} Nu_1(\xi)\,d\xi. \tag{31}$$

Figure 7(a) plots Q_1 as a function of the hump height h for $Pr = 0.7$. It is seen that as h increases Q_1 increases to a maximum value around $h = 1.25$ and then decreases. This may be explained by referring to the local wall heat flux distribution (Fig. 6(a)). As the height of the protrusion is increased, the local heat transfer rates increase on the windward side of the hump (except in a small region close to the leading edge) as the flow accelerates and convects heat away from the surface at a faster rate. However, the local heat transfer rates decrease on the leeward side of the hump as the flow decelerates, falling below the corresponding values for a flat plate. For protrusions with heights $h < 1.25$, the net effect is an enhancement in the total heat transfer rate. For humps of larger heights, the adverse pressure gradient induced on the leeward side of the hump slows down the flow to such an extent that the local heat transfer rates decrease considerably in that region. This leads to a decrease in the total heat transfer rate. The total heat transfer rate reaches a local minimum at $h \approx 3.0$. The flow first separates at $h \approx 1.9$. The region of separated flow is initially very small, and the fluid in the recirculating region moves very slowly. Heat transfer in this almost stagnant region is mainly by conduction. Locally, the separated region acts like an insulating layer, and the heat transfer rates are reduced. As h is increased, the size of the separated region increases and the fluid in the recirculating region begins to move faster. For $h > 3.0$, the induced mixing caused by the recirculation of fluid in the separated region leads to an increase in the total heat transfer rate. Since the current model is valid only for small-scale separation, the significance of the heat transfer enhancement due to the mixing induced by flow separation cannot be fully elucidated. The results, however, indicate the trend clearly. The enhancement of heat transfer due to boundary layer separation is seen more clearly in Fig. 7(b), which shows the variation of Q_1 with h for $Pr = 8$.

REFERENCES

1. K. Stewartson and P. G. Williams, Self-induced separation, *Proc. R. Soc. London* **A312,** 181–206 (1969).
2. A. F. Messiter, Boundary layer flow near the trailing edge of a flat plate, *SIAM J. Appl. Math.* **18,** 241–257 (1970).
3. V. Ya Neiland, Towards a theory of separation of the laminar boundary layer in a supersonic stream, *Izv. Akad. Nauk SSSR Mekh. Zhidk. Gaza* **4,** 53–57 (1969). Translation in *Fluid Dyn.* **4,** 33–35 (1969).
4. F. T. Smith, Laminar flow over a small hump on a flat plate, *J. Fluid Mech.* **57,** 803–824 (1973).
5. R. I. Sykes, Stratification effects in boundary layer flow over hills, *Proc. R. Soc. London* **A361,** 225–243 (1978).
6. O. R. Burggraf and P. W. Duck, Spectral computation of triple-deck flows. In *Numerical and Physical Aspects of Aerodynamic Flows*, pp. 145–158. Springer, Berlin (1981).
7. L. S. Yao, C. L. Tien and S. A. Berger, Thermal analysis of a fast moving slab in two adjacent temperature chambers, *J. Heat Transfer* **98,** 327–329 (1976).
8. A. F. Messiter and A. Linan, The vertical plate in laminar free convection: effects of leading and trailing edges and discontinuous temperature, *J. Appl. Math. Phys. (ZAMP)* **27,** 633–651 (1976).
9. J. W. Cooley and J. W. Tukey, An algorithm for the machine calculation of complex Fourier series, *Math. Comp.* **19,** 297–301 (1965).
10. C. Canuto, M. Y. Hussaini, A. Quarteroni and T. A. Zang, *Spectral Methods in Fluid Dynamics*. Springer, Berlin (1988).
11. F. T. Smith and K. Stewartson, On slot injection into a supersonic laminar boundary layer, *Proc. R. Soc. London* **A332,** 1–22 (1973).
12. F. T. Smith, Boundary layer flow near a discontinuity in wall conditions, *J. Inst. Math. Applic.* **13,** 127–145 (1974).

TRANSFERT THERMIQUE AUTOUR D'UNE PETITE PROTUBERANCE CHAUDE SUR UNE PLAQUE

Résumé—On présente les résultats d'une étude à nombre de Reynolds élevé du transfert thermique convectif autour d'une petite protubérance chaude sur une plaque plane. On analyse des excroissances de hauteur $\sim L\,Re^{-5/8}$ et de longueur $\sim L\,Re^{-3/8}$. Une solution analytique pour le transfert thermique est présentée pour des protubérances de hauteur extrêmement petite. Pour des hauteurs ~ 1 sur l'échelle de triple pont, on obtient une solution numérique. L'effet de la séparation de la couche limite sur le flux thermique transféré est étudié. On trouve que la séparation de l'écoulement conduit à des flux thermiques élevés en aval du point de séparation.

WÄRMEÜBERTRAGUNG IN DER UMGEBUNG EINER KLEINEN ERHEBUNG AUF EINER PLATTE

Zusammenfassung—Der konvektive Wärmeübergang bei hohen Reynolds-Zahlen an einer kleinen beheizten Erhebung auf einer ebenen Platte wird untersucht. Mit Hilfe der "Triple-Deck-Theory" werden Erhebungen der Höhe $\sim L\,Re^{-5/8}$ und der Länge $\sim L\,Re^{-3/8}$ analysiert. Eine analytische Lösung für den örtlichen Wärmeübergang wird für den Fall einer verschwindend kleinen Höhe der Erhebung vorgestellt. Für Erhebungen der relativen Höhe ~ 1 wird eine numerische Lösung ermittelt. Der Einfluß einer Grenzschichtablösung auf den Wärmeübergang wird untersucht, wobei sich stromab vom Ablösungspunkt besonders hohe örtliche Wärmeübergangskoeffizienten ergeben.

ТЕПЛОПЕРЕНОС ОКОЛО НЕБОЛЬШОГО НАГРЕВАЕМОГО ВЫСТУПА НА ПЛАСТИНЕ

Аннотация—Представлены результаты исследования конвективной теплоотдачи от небольшого нагреваемого выступа на плоской пластине при высоких числах Рейнольдса. С использованием теории трех уровней анализируются выступы высотой $\sim L\,Re^{-5/8}$ и длиной $\sim L\,Re^{-3/8}$. Предложено аналитическое решение для локальной интенсивности теплоотдачи для выступов с исчезающе малой высотой. Для выступов высотой ~ 1 в измеренном масштабе теории трех уровней получено численное решение. Исследуется влияние отрыва пограничного слоя на интенсивность теплопередачи. Найдено, что отрыв потока приводит к высокой локальной интенсивности теплопередачи вниз по течению от точки отрыва.